

Article

Comparative Study of Strategies for Enhancing the Performance of $\text{Co}_3\text{O}_4/\text{Al}_2\text{O}_3$ Catalysts for Lean Methane Combustion

Andoni Choya , Beatriz de Rivas, Jose Ignacio Gutiérrez-Ortiz and Rubén López-Fonseca * 

Chemical Technologies for Environmental Sustainability Group, Department of Chemical Engineering, Faculty of Science and Technology, University of the Basque Country UPV/EHU, P.O. Box 644, E-48080 Bilbao, Spain; andoni.choya@ehu.es (A.C.); beatriz.derivas@ehu.es (B.d.R.); joseignacio.gutierrez@ehu.es (J.I.G.-O.)

* Correspondence: ruben.lopez@ehu.es; Tel.: +34-94-601-5985

Received: 19 June 2020; Accepted: 7 July 2020; Published: 8 July 2020



Abstract: Spinel-type cobalt oxide is a highly active catalyst for oxidation reactions owing to its remarkable redox properties, although it generally exhibits poor mechanical, textural and structural properties. Supporting this material on a porous alumina can significantly improve these characteristics. However, the strong cobalt–alumina interaction leads to the formation of inactive cobalt aluminate, which limits the activity of the resulting catalysts. In this work, three different strategies for enhancing the performance of alumina-supported catalysts are examined: (i) surface protection of the alumina with magnesia prior to the deposition of the cobalt precursor, with the objective of minimizing the cobalt–alumina interaction; (ii) coprecipitation of cobalt along with nickel, with the aim of improving the redox properties of the deposited cobalt and (iii) surface protection of alumina with ceria, to provide both a barrier effect, minimizing the cobalt–alumina interaction, and a redox promoting effect on the deposited cobalt. Among the examined strategies, the addition of ceria (20 wt % Ce) prior to the deposition of cobalt resulted in being highly efficient. This sample was characterized by a notable abundance of both Co^{3+} and oxygen lattice species, derived from the partial inhibition of cobalt aluminate formation and the insertion of Ce^{4+} cations into the spinel lattice.

Keywords: cobalt oxide; methane oxidation; modified alumina; magnesium oxide; nickel cobaltite; ceria; lattice distortion; oxygen mobility

1. Introduction

The commercialization of vehicles driven by natural gas engines is a widely accepted strategy to mitigate the emissions associated with transport, which is one of the largest emitting sectors of greenhouse effect gases, due to their reduced CO_2 , NO_x , particles and hydrocarbons emissions [1,2]. However, the consolidation of this type of vehicles in the automotive fleet requires the control of the residual (around 1%) unburned methane (the main component of natural gas) emissions from the engine, since this pollutant possesses a powerful greenhouse effect potential (around 25 times that of CO_2 in a 100 years period). Owing to the high chemical stability of this compound and its low concentration in the flue gases (<1% vol.), the low-temperature catalytic oxidation appears as an attractive solution for this purpose. In order for this treatment not to significantly increase the cost of the engine, the selected catalyst must present a high activity with a reasonable economic investment.

Traditionally, the most commonly applied catalysts have been based on noble metals such as palladium or platinum [3,4]. However, this type of catalyst is generally expensive, due to the high cost of the noble metals and their relatively high metallic loading (2–4 wt %), and is prone to deactivation by sintering [5,6]. Spinel oxides based on transition metals can be a promising catalytic system for

the oxidation of lean methane, due to their lower cost, higher availability and relatively good activity for the oxidation of CO and light hydrocarbons [7,8]. More specifically, bulk spinel-type cobalt oxide (Co_3O_4) is regarded as a highly interesting substitute to noble metals for catalytic oxidation of trace amounts of methane on the basis of its excellent redox properties [9–12]. However, when prepared by conventional synthesis methodologies [13,14], the textural and structural properties of this oxide tend to be poor. Although some routes can partially overcome this problem, they are normally too complex and difficult to scale up to the industrial operation [15,16].

One possible alternative could be to use a porous media as a support for cobalt oxide, in order to increase the amount of active surface area available for reaction. This generally translates into an enhancement of the physico-chemical properties of the resulting catalyst, but the probability of the occurrence of a strong cobalt–support interaction, causing a negative effect on the redox properties of the deposited cobalt, is high. More specifically, when the selected support is high surface gamma alumina, this interaction provokes the formation of a cobalt aluminate phase (CoAl_2O_4), which is characterized by a poor reducibility and a consequent low specific activity for oxidation reactions [17,18].

A proposed solution would be the modification of the properties of the alumina with the aim of tuning its affinity for the Co_3O_4 deposited over it. This can be carried out by incorporating some chemical promoters to the alumina before the deposition of Co_3O_4 , or by adding the promoters after the formation of the final $\text{Co}/\text{Al}_2\text{O}_3$ catalyst. In this sense, Liotta et al. [19] reported that adding Ba during the sol–gel synthesis of Al_2O_3 decreased diffusion of the Co^{2+} ions into the structure of the alumina after Co deposition. Similarly, Park et al. [20] and Park et al. [21], on different studies, observed that adding phosphorus to Al_2O_3 resulted in the formation of a mixed AlPO_4 phase that partially suppressed the formation of CoAl_2O_4 . On the other hand, Cheng et al. [22] found out that the addition of Mn or Fe during the synthesis of a $\text{Cu-Co}/\text{Al}_2\text{O}_3$ catalyst improved the redox properties of both active metals. In addition, El-Shobaky et al. [23] reported an increased activity for CO oxidation of $\text{Co}_3\text{O}_4/\text{Al}_2\text{O}_3$ catalysts doped with small amounts of Mn and/or La.

Similarly, an attractive strategy to improve the performance of this type of catalyst could be using magnesium as a modifier. In this sense, Riad [24] observed that alumina coated with magnesium and prepared by coprecipitation presented better properties than bare alumina. Cobalt catalysts can also be supported over pure magnesium oxide, which results in systems with enhanced activity due to the magnesium–cobalt interaction, as reported by Ulla et al. [25] and Ji et al. [26].

Considering this background, in the present paper various enhancing strategies for γ -alumina-supported cobalt catalysts were examined in order to determine their efficiency for improving the activity of the resulting catalysts for the complete oxidation of methane under lean conditions with respect to an unmodified reference $\text{Co}/\text{Al}_2\text{O}_3$ catalyst (Co/Al sample). The three investigated approaches were the following:

- (i) Superficial protection of alumina with magnesia prior to the deposition of cobalt (Co/Mg-Al sample). The cobalt content was fixed at 30 wt % and the Mg/Co molar was 0.25.
- (ii) Co-deposition of nickel and cobalt over alumina in order to promote the redox properties of Co_3O_4 (Co-Ni/Al sample). Since nickel oxide can show a significant activity of methane oxidation [27,28], the total metallic loading was fixed at 30 wt % while using a Ni/Co molar ratio of 0.20.
- (iii) Coating the alumina surface with ceria before the addition of cobalt in order to eventually serve as both a surface protector for alumina and redox promoter for cobalt oxide (Co/Ce-Al sample). The cobalt content was fixed at 30 wt % and the Ce/Co molar was 0.20.

2. Results

2.1. Physico-Chemical Characterization

Along with their chemical composition as determined by Wavelength dispersive X-ray fluorescence (WDXRF), the textural properties of the synthesized catalysts in terms of the BET (Brunauer–Emmett–Teller) surface and pore volume are listed in Table 1. Additionally, the properties of

bare alumina and the modified supports with MgO and CeO₂ are included for comparative purposes. All supports and catalysts exhibited type IV adsorption–desorption isotherms (Figure 1) with H2 type hysteresis cycles, characteristic of mesoporous materials with a relatively broad size distribution. The addition of ceria provoked an appreciable decrease (16%) in the surface area whereas the effect of MgO deposition was virtually negligible. After incorporating the active metallic oxide, the surface area decreased by around 19–32%. Hence, the specific surface area of the catalysts varied in the 93–113 m² g⁻¹ range while the pore volume was between 0.27 and 0.35 cm³ g⁻¹.

Table 1. Physico-chemical properties of the supported cobalt catalysts.

Sample	Co Loading, wt %	Me Loading, wt %	Me/Co Molar Ratio	BET Surface, m ² g ⁻¹	Pore Volume, cm ³ g ⁻¹	Cophase Crystallite Size, nm
Al ₂ O ₃	-	-	-	139	0.56	-
Mg-Al	-	6.7	-	145	0.50	-
Ce-Al	-	20.6	-	117	0.42	-
Co/Al	27.9	0.0	0	108	0.29	29
Co/Mg-Al	28.7	3.0	0.25	99	0.27	23
Co-Ni/Al	23.2	4.8	0.21	113	0.35	21
Co/Ce-Al	29.5	12.4	0.18	93	0.30	23

Me stands for Mg, Ni or Ce.

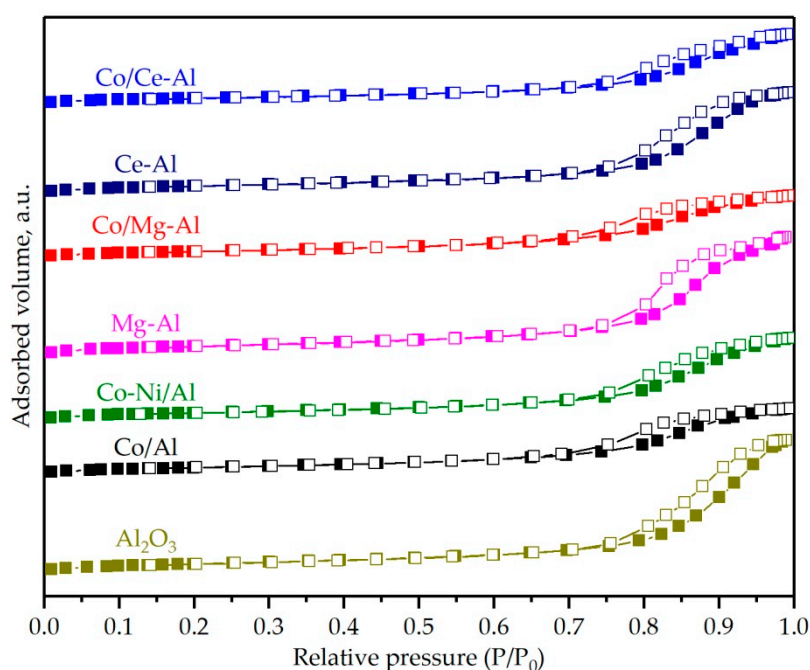


Figure 1. N₂ physisorption isotherms of the supported cobalt catalysts.

The pore size distributions of the supports and the cobalt catalysts are shown in Figure 2. The blank alumina exhibited a bimodal distribution with maxima at 110 and 150 Å, while the distributions were unimodal, centered at 110 Å, over the MgO- and CeO₂ modified supports, thereby showing that the promoter oxides were preferentially deposited on the larger pores of the alumina. On the other hand, all cobalt catalysts exhibited unimodal distributions centered at 90 Å, thus evidencing that cobalt was also massively located on the larger pores of the supports.

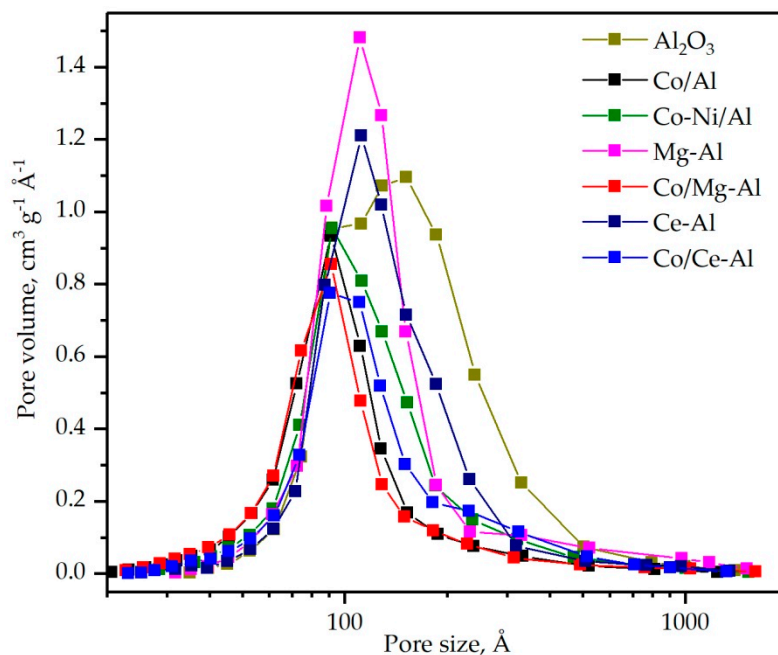


Figure 2. Pore size distributions of the supported cobalt catalysts.

The structural characterization of the catalysts was performed by XRD. The diffractograms in Figure 3 revealed signals of a cubic spinel phase ($2\theta = 19.1^\circ, 31.3^\circ, 37.0^\circ, 45.1^\circ, 59.4^\circ$ and 65.3°) in the four cobalt catalysts that could be assigned to the presence of both Co_3O_4 (ICDD 00-042-1467) and CoAl_2O_4 (ICDD 00-044-0160) formed by the interaction of the deposited cobalt with the alumina [29,30]. The relative occurrence of these two phases could not be determined since both oxides essentially exhibit the same diffraction signals at similar positions.

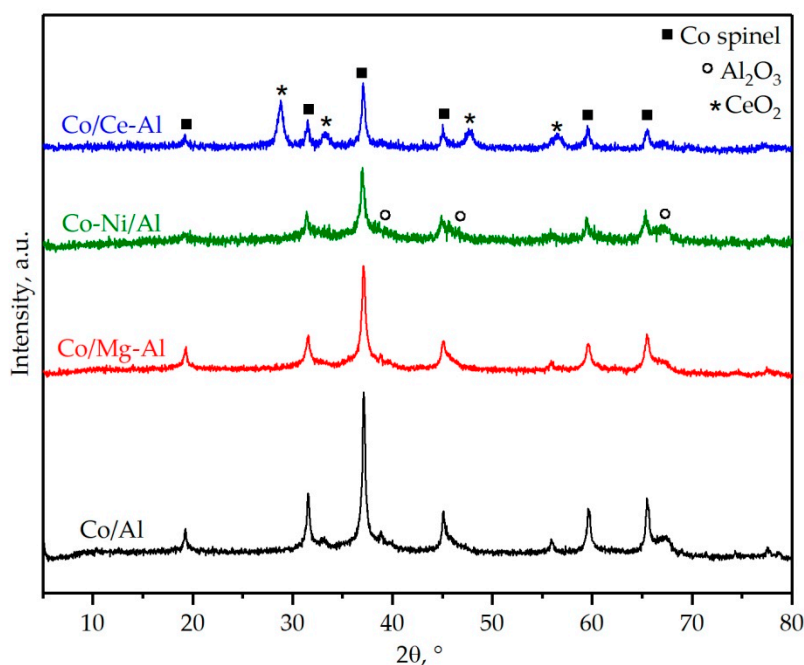


Figure 3. XRD patterns of the supported cobalt catalysts.

On the other hand, weak signals from a cubic phase with low crystallinity were detected at $2\theta = 37.7^\circ, 45.9^\circ$ and 66.9° that could be attributed to the gamma-alumina (ICDD 01-074-2206). Additionally, various signals from a fluorite-like phase of CeO_2 were detected at $2\theta = 28.5^\circ, 33.3^\circ, 47.5^\circ$ and 56.4° for

the Co/Ce-Al catalyst. Due to the lower amount of Mg and Ni (<5 wt %), no signals attributable to MgO and NiO were noticed over the Co/Mg-Al and the Co-Ni/Al samples, respectively.

The average crystallite size of the cobalt spinel phase was estimated from the full width half maximum (FWHM) of the characteristic peak located at 37.1° , assignable to the (311) crystalline plane, by applying the Scherrer equation (Table 1). The crystallite size for the catalyst supported over bare alumina was 29 nm, while it was slightly smaller (21–23 nm) over the modified catalysts. It must be noted that sizes calculated from the refinement were not substantially different from those obtained from single peak data. Furthermore, a close-up view of this signal (Figure 4) revealed a significant 2θ shift towards lower angle values, thus denoting an enlargement of the cell size of the spinel due to the insertion of cations of the promoters into its lattice. In this sense, the Co-Ni/Al catalyst showed the largest growth ($a_0 = 8.122 \text{ \AA}$) with respect to the catalyst supported over bare alumina ($a_0 = 8.096 \text{ \AA}$). This remarkable growth may indicate the presence of the nickel cobaltite mixed spinel (NiCo_2O_4) in this sample [28,31].

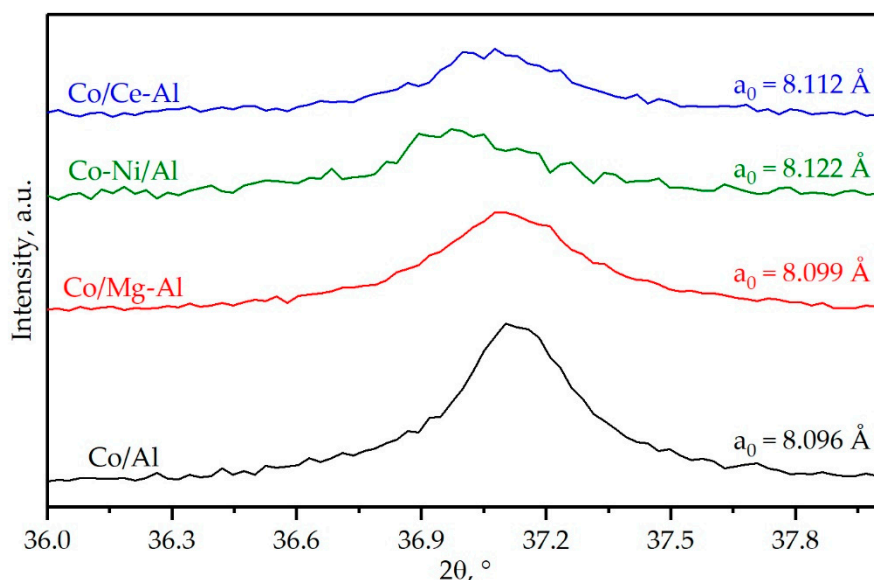


Figure 4. Close up view of the XRD patterns of the supported cobalt catalysts in the $2\theta = 36\text{--}38^\circ$ range.

A closer inspection of the position and width of the A_{1g} mode of the modified catalysts could be helpful in determining a possible distortion of the Co_3O_4 lattice due to the insertion of cations of the promoters. This influence was analyzed in terms of the shift and the FWHM value of this signal (Figure 5). The shift of the A_{1g} signal of the modified catalysts with respect to the reference Co/Al sample ranged between 4 and 17 cm^{-1} , with the Co-Ni/Al catalyst exhibiting the largest shift. In addition, the FWHM for the modified catalysts was between 26 and 30 cm^{-1} , while it was 13 cm^{-1} for the unmodified catalyst. These results revealed that the most marked lattice distortion occurred over the Co-Ni/Al catalyst, in line with the results from XRD. However, the Raman spectra of this sample did not show any detectable signals related to the presence of NiCo_2O_4 in contrast to what was observed over the enlargement of the cell size of the crystalline spinel phase suggested. Therefore, the amount of nickel cobaltite present in this catalyst was probably low.

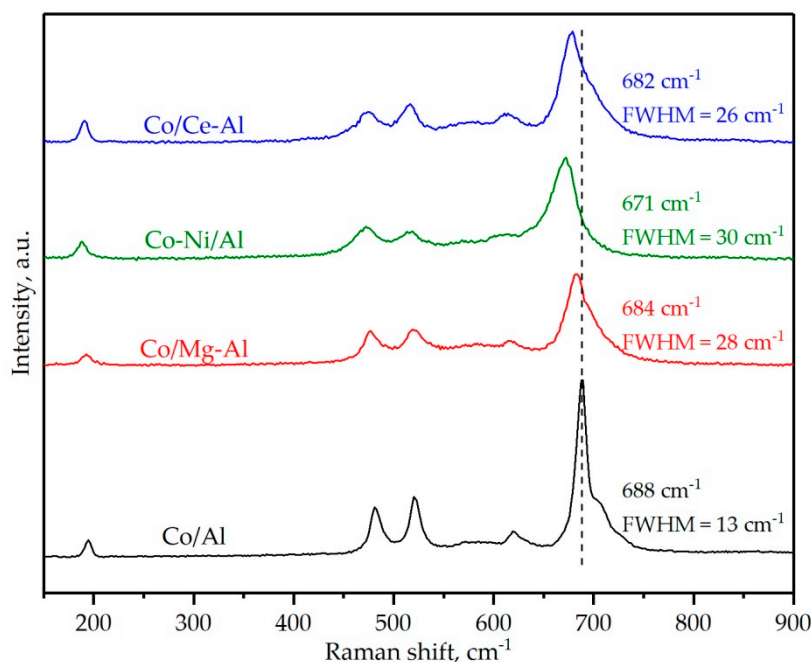


Figure 5. Raman spectra of the supported cobalt catalysts.

Figure 6 shows the $\text{Co}2p_{3/2}$ XPS spectra of the samples. The spectra of all catalysts were composed of five different signals. As for the Co/Al sample the two features with the lowest binding energies, located at 779.5 and 781.0 eV, were assigned to Co^{3+} and Co^{2+} ions, respectively, while the signal centered at 783.2 eV was attributed to the presence of CoO in the surface of the samples [32,33]. The two signals with the highest binding energies (786.2 and 790.1 eV) were identified as the satellite signals from Co^{3+} and Co^{2+} ions, respectively. The position of the main signal of the $\text{Co}2p_{3/2}$ spectra can be used as an indication of the predominant cobalt species on the surface of each sample. Thus, higher binding energy values suggested a higher abundance of Co^{2+} cations, while lower binding energies pointed out a favored presence of Co^{3+} cations. In this sense, the position of the main signal of the unmodified catalyst was 781.1 eV, thereby evidencing a significant presence of Co^{2+} ions, in line with its higher CoAl_2O_4 content as deduced by Raman spectroscopy. Conversely, the main signal for the Co/Mg-Al sample was centered at 780.8 eV assignable to a slightly lower Co^{2+} content. This observation was not coherent with the results from Raman spectroscopy that evidenced that the presence of CoAl_2O_4 in this sample was appreciably limited. For this reason, the increased Co^{2+} presence was not attributed to the presence of cobalt aluminate, but rather to the probable formation of a Co-Mg solid solution, as already reported elsewhere [34,35].

On the other hand, the main signals of the Co-Ni/Al and Co-Ce/Al catalysts exhibited a significant shift towards lower binding energies with respect to the Co/Al sample. Thus, both catalysts displayed their main signal centered at about 780.1 eV, thus evidencing their higher content in Co^{3+} cations. Additionally, the $\text{Ni}2p_{3/2}$ spectra of the Co-Ni/Al catalyst (not shown) were deconvoluted into five signals. Hence, three main contributions at 853.7, 855.3 and 857.3 eV were attributed to the presence of Ni^{2+} as NiO, Ni^{2+} belonging to a spinel lattice and Ni^{3+} cations, respectively, while the signals at 861.2 and 866.5 eV were assigned to the satellites of Ni^{2+} and Ni^{3+} cations, respectively. The relatively low binding energy of the signal associated with the presence of Ni^{2+} cations in a spinel lattice (855.3 eV) also denoted that these species were mainly a part of the NiCo_2O_4 spinel instead of the NiAl_2O_4 , for which the binding energy of that signal would be expectedly higher (ca. 856.0 eV), as shown by other studies [36,37].

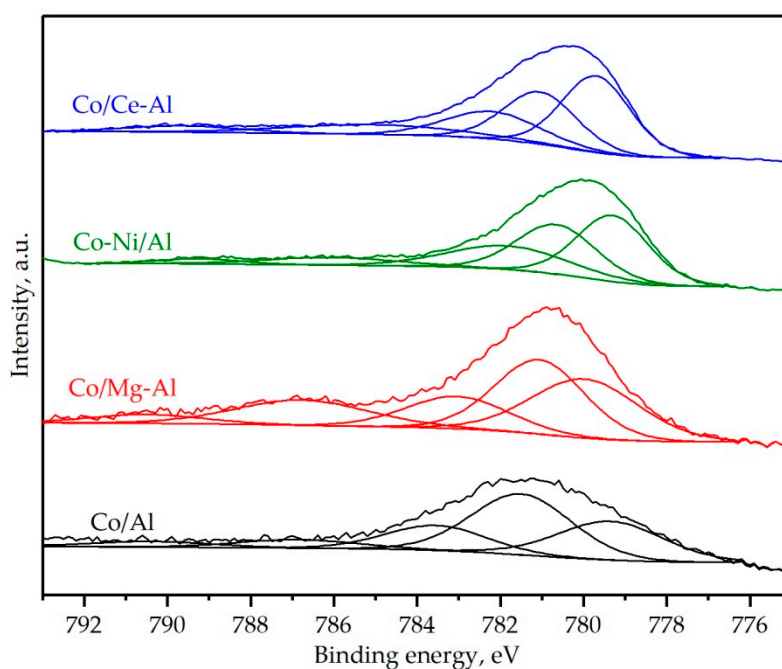


Figure 6. Co_{2p_{3/2}} XPS spectra of the supported cobalt catalysts.

The deconvolution and integration of the XPS spectra allowed for a quantitative analysis of the composition of the surface, as shown in Table 2. Firstly, it must be noticed that the surface cobalt loading of the Co/Al sample and particularly Co/Mg-Al sample was significantly lower than their bulk content, which, on one hand, suggested that a notable fraction of Co species was as CoAl₂O₄ and, on the other hand, evidenced a marked formation of the aforementioned Co-Mg solid solution. These results would be in agreement with the relatively low Co³⁺/Co²⁺ molar ratios of these catalysts (0.67 and 0.94, respectively).

Table 2. Surface composition of the supported cobalt catalysts.

Catalyst	Co, wt %	Me, wt %	Co ³⁺ /Co ²⁺ Molar Ratio	O _{ads} /O _{latt} Molar Ratio
Co/Al	22.6 (27.9)	-	0.67	1.41
Co/Mg-Al	13.3 (28.7)	4.4 (3.0)	0.94	1.02
Co-Ni/Al	25.4 (23.2)	8.2 (4.8)	1.21	0.94
Co/Ce-Al	32.9 (29.5)	3.2 (12.4)	1.38	0.77

The values in brackets correspond to the bulk composition. Me stands for Mg, Ni or Ce.

On the other hand, a substantial surface cobalt enrichment was noticed for the Co-Ni/Al and Co/Ce-Al catalysts, thus pointing out that deposited cobalt was preferentially located on the external surface and it did not tend to strongly interact with the support. This in turn was in good agreement with the higher Co³⁺/Co²⁺ molar ratios of these samples (1.21 and 1.38, respectively). It is worth pointing out that this higher abundance of Co³⁺ species at the surface was accompanied by a more notable presence of lattice oxygen species in the Co-Ni/Al and Co/Ce-Al catalysts, as shown in Table 2. This type of oxygen species is usually involved in the oxidation of methane by a Mars-van Krevelen mechanism [38,39]. As revealed by our results, its abundance was optimized over the Co/Ce-Al catalyst. It is quite reasonable to expect that the Ce³⁺/Ce⁴⁺ relative abundance can play a role in controlling the activity of the Co/Ce-Al. Unfortunately, since the amount of Ce at the surface of the catalyst is very low, a proper deconvolution of the Ce3d XPS spectrum devoted to the evaluation of the Ce³⁺/Ce⁴⁺ molar ratio was not possible. In this sense, we have shown elsewhere [40] that an inverse relationship between the Ce³⁺/Ce⁴⁺ and the Co³⁺/Co²⁺ molar ratios, as determined by XPS, for a series of Ce-doped bulk Co₃O₄ catalysts with a Ce/Co molar ratio between 0.03 and 0.14 (corresponding to 5–20 wt % Ce).

These results could be explained in terms of the equilibrium $\text{Ce}^{3+} + \text{Co}^{3+} \leftrightarrow \text{Ce}^{4+} + \text{Co}^{2+}$, established by the requirement of charge balance within the cations of the spinel lattice. Since our XRD and Raman measurements suggested the insertion of Ce cations into the Co_3O_4 lattice in the Co/Ce-Al sample, the aforementioned effect could also be occurring in this catalyst. This would explain the higher surface $\text{Co}^{3+}/\text{Co}^{2+}$ molar ratio among all the samples.

The redox properties of the cobalt catalysts were investigated by temperature-programmed reduction with hydrogen (H_2 -TPR) and temperature-programmed reaction with methane in the absence of oxygen (CH_4 -TPRe). As widely accepted, the H_2 -TPR profile of the base alumina-supported Co_3O_4 catalyst (Figure 7) evidenced a two-step reduction process [41,42]. A first H_2 uptake at low temperatures (<550 °C) was associated with the reduction of Co_3O_4 , which in turn could be subdivided into two contributions located at around 270–310 °C, assignable to the reduction of Co^{3+} ions into Co^{2+} , and at 350–400 °C, attributable to the subsequent reduction of Co^{2+} into metallic cobalt. This second H_2 uptake did not take the shape of a single peak, but instead was formed of at least two different contributions, which suggested the presence of Co^{2+} species with varying reducibilities. The presence of this type of species was much more noticeable for the Co/Mg-Al catalysts, where the temperature window for this second reduction event extended from 300 to 550 °C. On the other hand, the marked H_2 consumption located at high temperatures (>600 °C) over the four catalysts was attributed to the reduction of cobalt aluminate [43].

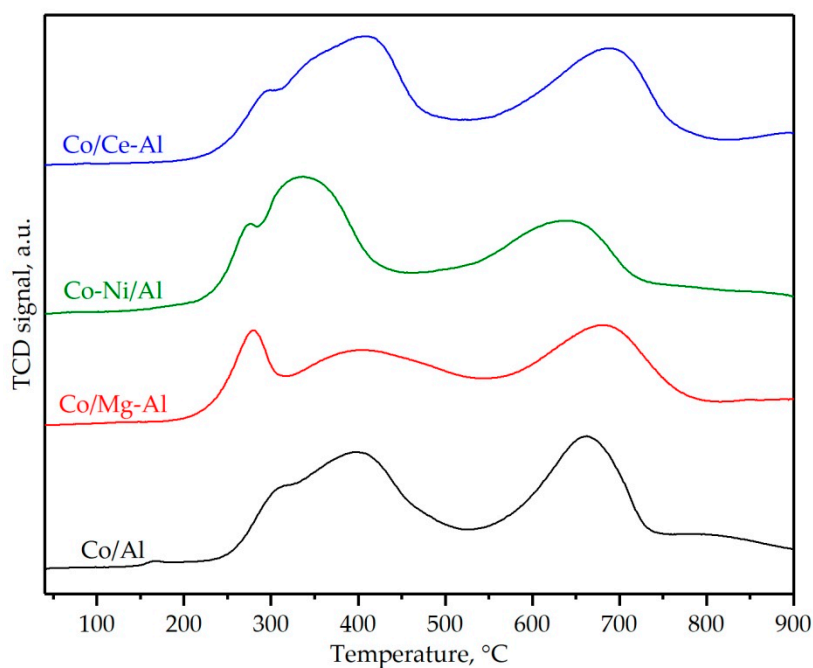


Figure 7. Temperature-programmed reduction with hydrogen (H_2 -TPR) profiles of the supported cobalt catalysts.

The relative amount of each type of Co species present in the various catalysts was estimated by deconvolution of the experimental TPR profiles. The threshold temperature of 550 °C was taken as a criterion to distinguish between easily reducible cobalt species (low-temperature uptake), namely free Co_3O_4 (200–450 °C) and some mixed cobalt-metal species (450–550 °C) such as cobalt-magnesium species, and hardly reducible cobalt species (high-temperature uptake) in the form of cobalt aluminate (>550 °C). The results are summarized in Table 3.

Table 3. Characterization by H₂-TPR and temperature-programmed reaction with methane in the absence of oxygen (CH₄-TPRe) of the supported cobalt catalysts.

Catalyst	H ₂ -TPR		Onset Reduction Temperature, °C	CH ₄ -TPRe
	Low-Temperature H ₂ Uptake, mmol g _{Co} ⁻¹	High-Temperature H ₂ Uptake, mmol g _{Co} ⁻¹		Low-Temperature O ₂ Consumption, mmol g _{Co} ⁻¹
Co/Al	9.8	10.2	225	0.28
Co/Mg-Al	10.3	10.4	195	0.61
Co-Ni/Al	12.5	12.9	175	0.83
Co/Ce-Al	13.6	8.5	220	0.88

Firstly, it must be noticed that the H₂ uptake at low temperatures, associated with species with a high reducibility, mainly free of Co₃O₄, was larger for the three modified catalysts with respect to the Co/Al sample. The increase in H₂ uptake was 5% for the Co/Mg-Al, 28% for the Co-Ni/Al and 39% for the Co/Ce-Al, thus showing that nickel and cerium were efficient redox promoters for cobalt. On one hand, for the Co-Ni/Al catalyst, the increase in H₂ uptake at a low temperature could be due to the presence of the NiCo₂O₄ spinel, which possesses a higher specific H₂ uptake than Co₃O₄. On the other hand, for the Co/Ce-Al sample, the increase could be related to the reduction of the surface of the ceria, which is known to occur at around 450–500 °C [44], and also the improved reducibility of cobalt oxide due to the insertion of cerium cations into its lattice. Additionally, the onset reduction temperature of the three modified catalysts was clearly lowered. The most noticeable temperature shift occurred for the catalyst modified with nickel (50 °C), which could be due to the presence of nickel cobaltite, while it was much less significant for the Co/Ce-Al catalyst (5 °C).

On the other hand, the H₂ uptake assignable to the presence of CoAl₂O₄ was only lower for the Co/Ce-Al catalyst (8.5 mmol g_{Co}⁻¹) with respect to the Co/Al sample (10.2 mmol g_{Co}⁻¹); while it was notably higher (12.9 mmol g_{Co}⁻¹) over the Co-Ni/Al catalyst. This could be due to ceria acting as a physical barrier between cobalt and alumina, whereas both cobalt and nickel were directly deposited on the alumina in the case of the Co-Ni/Al sample. Therefore, the cobalt–alumina interaction was not apparently limited over this sample. Alternatively, given that the Co/Mg-Al catalyst showed a comparable H₂ uptake at high temperatures (10.4 mmol g_{Co}⁻¹), it could be thought that such a barrier effect could be ruled out in this catalyst as well. However, it must be noticed that a certain fraction of this H₂ uptake would probably be due to the partial reduction of a Co-MgO solid solution. Therefore, the total H₂ uptake associated with the presence of cobalt aluminate was probably lower than that of the Co/Al sample.

As a complement of the H₂-TPR analysis, the reactivity of oxygen species present in the examined catalysts was also analyzed by temperature-programmed reaction with methane in the absence of oxygen (CH₄-TPRe). The evolution of evolved CO₂, CO and H₂ was monitored by mass spectrometry. In general, the CO₂ profiles evidenced a two-step reaction process, as depicted in Figure S1, Supplementary Material. The low-temperature reaction step was attributed to the complete oxidation of methane by lattice oxygen species associated with Co³⁺ ions. No CO or H₂ formation was detected at this temperature interval. The amount of CO₂ evolved from the complete oxidation reaction was barely perceptible over the Co/Al sample. Above 525–550 °C the methane partial oxidation occurred, where methane reacted with low-mobility oxygen species associated with Co²⁺ ions, yielding significant amounts of CO and H₂ along with CO₂ [14]. It must be noted that the occurrence of this second process was not observed over the Co/Al catalyst, thus suggesting that it could only take place at temperatures higher than 600 °C.

The comparatively larger formation of CO₂ above 500 °C made the proper analysis of the obtained results in the low-temperature range rather difficult. For this reason, Figure 8 only focuses on the evolution of the CO₂ yield between 100 and 550 °C. It was thus clearly evidenced that the three investigated enhancing strategies were efficient for increasing the amount of reactive oxygen in the resulting cobalt catalysts. More specifically, the O₂ consumption at low temperatures (Table 3) increased from 0.28 mmol g_{Co}⁻¹ for the Co/Al sample up to 0.61–0.88 mmol g_{Co}⁻¹ for the modified catalysts,

with the Co/Ce-Al achieving the highest value. Note that the amount of reacted O_2 was relatively limited over the Co/Mg-Al sample in spite of its higher Me/Co molar ratio (0.25). Additionally, this low-temperature step peaked at lower temperatures with respect to the reference cobalt catalyst. The temperature shift was as high as 67 °C for the Co-Ni/Al catalyst. Such remarkable improvement could be due to the presence of $NiCo_2O_4$ in this sample, which has been already reported to be highly reducible and active for methane oxidation elsewhere [27,45].

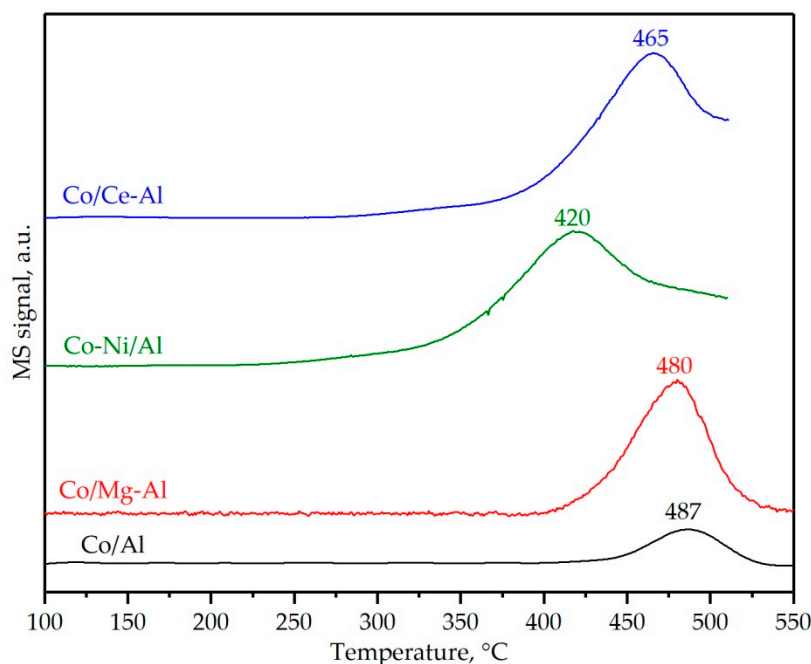


Figure 8. Close up view of the CH_4 -TPRe profiles of the supported cobalt catalysts in the 100–550 °C temperature range.

Given the notable redox behavior of the Co-Ni/Al and Co/Ce-Al catalysts, these were examined by high angle annular dark field—scanning transmission electronic microscopy (HAADF-STEM) coupled with electron energy loss spectroscopy (EELS) or energy dispersive X-ray spectrometry (EDX), respectively. Elemental maps (Figure 9 and Figure S2, Supplementary Material) were generated for certain areas in each sample to allow studying the spatial distribution of cobalt and nickel or cerium in the bimetallic catalysts. These results evidenced that both Ni and Ce were homogeneously present over the supported nanoparticles. In the case of nickel, this probably means that it was forming nickel cobaltite. The Co/Ce-Al sample also contained small nanoparticles of cerium species (as ceria) of around 10–20 nm.

2.2. Catalytic Performance

Three consecutive light-off tests were carried out for each catalyst. The second and third cycles were characterized by an identical light-off curve. Hence, the light-off curves corresponding to the third cycle of each catalyst are shown in Figure 10. It must be noticed that all four samples presented 100% selectivity towards CO_2 . It was clear that the three modified catalysts resulted were remarkably more efficient than the base Co/Al catalyst. In this sense, the corresponding T_{50} value (Table 4) was lowered by 15 (Co/Mg-Al), 50 (Co-Ni/Al) and 70 °C (Co/Ce-Al). Note that the intrinsic activity of the Co-free alumina supports (pure Al_2O_3 , Mg-Al and Ce-Al) was negligible at 600 °C.

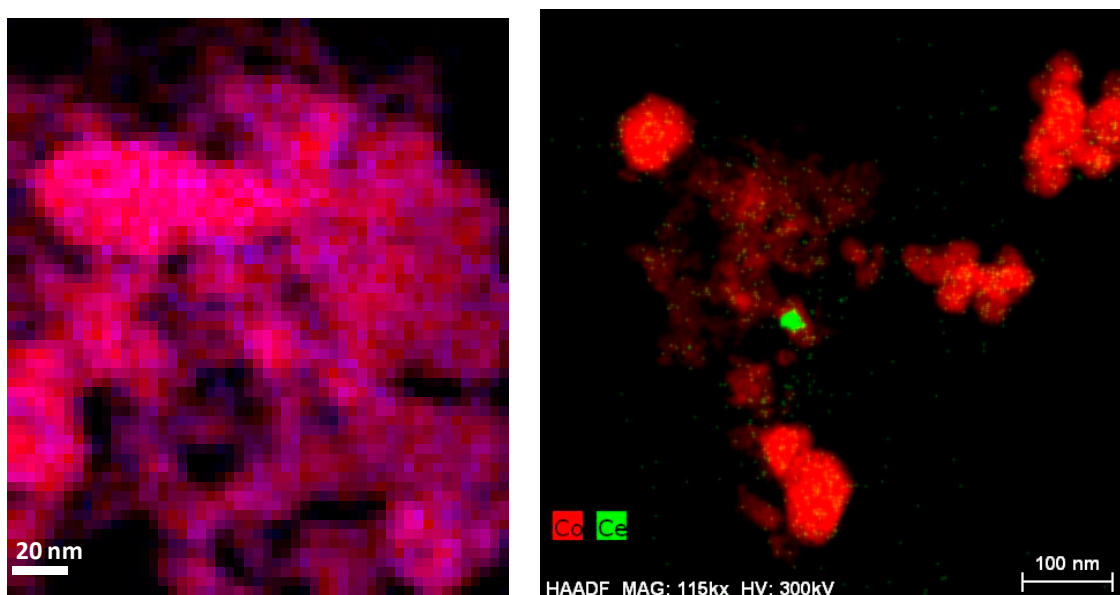


Figure 9. High angle annular dark field–scanning transmission electron microscopy (HAADF–STEM) images of the Co-Ni/Al (**left**) and Co/Ce-Al (**right**) catalysts coupled to electron energy loss spectroscopy (EELS; Co (red) and Ni (blue)) and energy dispersive X-ray spectrometry (EDX; Co (red) and Ce (green)) elemental distribution.

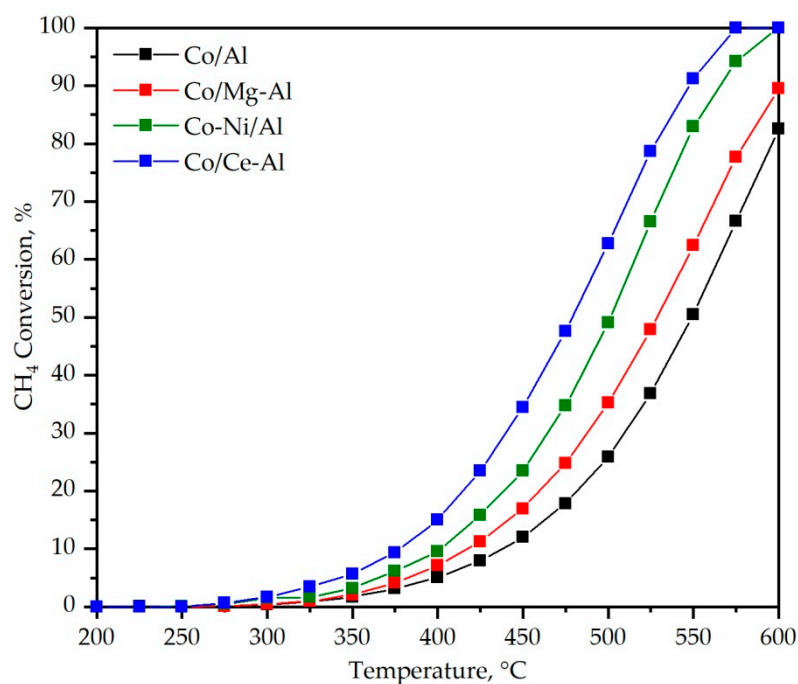


Figure 10. Light off curves of the supported cobalt catalysts.

Table 4. Kinetic results of the supported cobalt catalysts.

Catalyst	T_{50} , °C	Specific Reaction Rate at 400 °C, $\text{mmol g}_{\text{Co}}^{-1} \text{h}^{-1}$	E_a , kJ mol^{-1}
Co/Al	550	1.2	82 ± 2
Co/Mg-Al	535	1.5	83 ± 2
Co-Ni/Al	500	2.5	84 ± 2
Co/Ce-Al	480	3.2	80 ± 2

The apparent activation energy of the four evaluated catalysts (Table 4) were estimated by the integral method, assuming that the reaction kinetics followed a pseudo-order one for methane and a zeroth order for oxygen, as it is usual for the Mars–van Krevelen mechanism in the presence of excess oxygen [46,47]. The corresponding linearized plots are depicted in Figure S2. The activation energies were around 80–84 kJ mol⁻¹, a value comparable to those reported in other studies for methane oxidation over Co₃O₄-based catalysts [48,49]. Thus, it could be concluded that the main active species in all four catalysts was free of Co₃O₄.

On the other hand, the specific reaction rates of the various catalysts were estimated by the differential method (for methane conversions lower than 20%). In this analysis, for the sake of proper comparison, the specific activity of the various catalysts were calculated at the same temperature (400 °C) and normalized per gram of cobalt. The results are shown in Table 4. All three modified samples achieved higher reaction rates (1.5–3.2 mmol CH₄ g_{Co}⁻¹ h⁻¹) with respect to the unmodified counterpart (1.2 mmol CH₄ g_{Co}⁻¹ h⁻¹). The catalyst promoted with ceria (Co/Ce-Al), in particular, presented the highest reaction rate, which was almost three times higher than that of the catalyst supported over bare alumina.

In view of these results, modifying the alumina support with ceria prior to the deposition of cobalt would be a quite promising strategy to be developed for improving the activity of cobalt catalysts. Interestingly, when cobalt was deposited over the Ce-modified support, a dual beneficial effect was evidenced. On one hand, ceria was found to act as a physical barrier between alumina and deposited cobalt, limiting the cobalt–alumina interaction and the subsequent cobalt aluminate formation. On the other hand, the interaction between cobalt and ceria led to a partial incorporation of cerium ions into the lattice of Co₃O₄. Both phenomena in turn led to a larger abundance of Co³⁺ and therefore to a promoted mobility of the lattice oxygen species at low temperatures with ceria loading as shown in Figure 11.

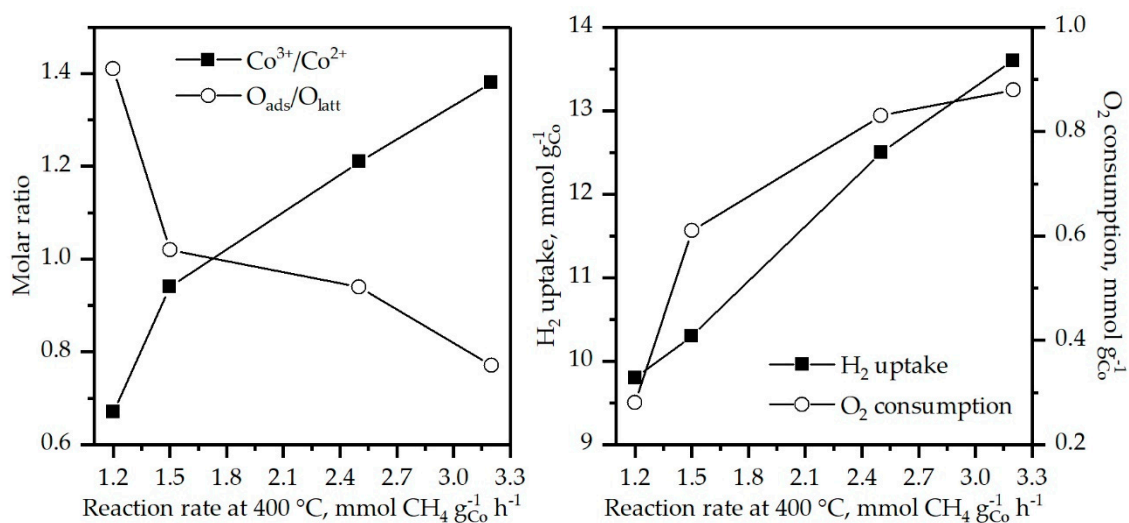


Figure 11. Relationship among specific reaction rate and: surface Co³⁺/Co²⁺ and O_{ads}/O_{latt} molar ratios (left); low-temperature H₂ uptake from H₂-TPR and low-temperature O₂ consumption from CH₄-TPRe (right).

3. Materials and Methods

3.1. Catalyst Preparation

A commercial γ -alumina kindly provided by Saint Gobain was used as the base support. Alternatively, the alumina was modified with MgO (Mg-Al) or CeO₂ (Ce-Al), which were incorporated by precipitation, starting with magnesium nitrate and cerium nitrate, respectively, followed by a calcination step (600 °C for 4 h).

Four alumina supported cobalt oxide catalysts, namely Co/Al, Co-Ni/Al, Co/Mg-Al and Co/Ce-Al, were prepared following a simple precipitation route as detailed elsewhere [50]. This methodology consisted of the precipitation of aqueous solutions of cobalt nitrate hexahydrate and eventually nickel nitrate hexahydrate with adjusted concentrations by the drop-by-drop addition of a sodium carbonate 1.2 M solution at a constant temperature of 80 °C until pH 8.5 was achieved. Afterwards, the precipitates were thoroughly washed with deionized water in order to remove the residual sodium ions that are known to be detrimental for the activity of the resulting catalysts [40]. The washed precipitates were dried at 110 °C for 16 h and then subjected to calcination at 600 °C for 4 h in static air. The Me/Co molar ratio (where M = Mg, Ni or Ce) of the modified catalysts was 0.20 for the Co-Ni/Al and Co/Ce-Al samples and 0.25 for the Co/Mg-Al catalyst, as dictated from a previous optimization for this type of cobalt catalysts [51,52]. The total amount of active metal (Co and/or Ni) was fixed at 30 wt %.

3.2. Characterisation Techniques

Wavelength dispersive X-ray fluorescence (WDXRF) determined the composition of the synthesized catalysts. Previously, a boron pearl glass was obtained by mixing the corresponding catalyst with a commercial flux agent (Spectromelt A12) with a 1:20 mass ratio. This mixture was then melted at 1200 °C. Measurements were performed under vacuum with PANalytical AXIOS sequential WDXRF spectrometer equipped with a Rh tube and three different detectors (gas flow, scintillation and Xe sealed).

Specific surface area (BET method), pore volume (BJH method) and pore size distribution (BJH method) were estimated by low-temperature (−196 °C) N₂ physisorption with a Micromeritics TriStar II instrument. The samples were submitted to degassing before analysis with flowing N₂ in a Micromeritics SmartPrep sample preparation system at 300 °C for 10 h.

Powder X-ray diffraction (XRD) and Raman spectroscopy were used for the structural characterization of the cobalt catalysts. XRD data were collected on an X'PERT-PRO X-ray diffractometer using Cu K α radiation ($\lambda = 1.5406 \text{ \AA}$) and a Ni filter at 40 kV and 40 mA. The patterns were collected with the 2 θ range from 10 to 80° with a step size of 0.026° and a counting time of 2.0 s. The cell size of the Co-spinel phase was calculated by profile matching of the whole diffractogram using FullProf.2k software. Raman measurements were performed on a Renishaw InVia Raman spectrometer using a 514 nm laser source (ion-argon laser, Modu-Laser), scanning from 150 to 1200 cm^{−1}. For each analysis, 20 s were employed and 5 scans were accumulated.

X-ray photoelectron spectroscopy (XPS) was employed for characterizing the structure and chemical composition and the electronic structure at the surface level. The analysis was carried out with a SPECS system coupled to a Phoibos 150 1D analyzer and a DLD (Delay–Line Detector)-monochromatic radiation source.

The redox behavior of the cobalt catalysts was examined by temperature-programmed reduction with hydrogen (H₂-TPR) with a Micromeritics Autochem 2920 equipment with a 5% H₂/Ar stream. The samples were first conditioned at 300 °C for 30 min with a flowing 5% O₂/He mixture. Next, they were cooled down to 50 °C in an inert stream. The reduction process was conducted up to 600 °C with a heating rate of 10 °C min^{−1}. In addition, the reducibility of the samples was also examined by temperature-programmed reaction with methane (CH₄-TPRe) with a 5% CH₄/He mixture.

Elemental maps of Co, Ni and Ce were obtained by electron energy loss spectroscopy (EELS) or energy dispersive X-ray spectrometry (EDX), both in the scanning transmission electron microscopy—high angle annular dark field (STEM–HAADF) mode (FEI Titan Cubed operating at 300 kV and Philips CM200 operating at 200 kV), with a Tridiem Energy Filter (Gatan) and Super-X detector (ChemSTEM) as detectors, respectively. The Co-Ni/Al and Co/Ce-Al samples were characterized by EELS-STEM and EDS-STEM, respectively.

3.3. Catalytic Activity Determination

The catalytic performance was examined in a fixed bed reactor (Microactivity by PID Eng & Tech S.L., Alcobendas, Madrid). A multipoint K type thermocouple was fixed to the middle of the catalyst bed in order to control the reaction temperature. Of the catalyst 1 g (sieve fraction of 0.25–0.3 mm) diluted with 1 g of inert quartz (sieve fraction of 0.5–0.8 mm) was used. A gaseous mixture ($500 \text{ cm}^3 \text{ min}^{-1}$) of CH_4 (1 vol.%), O_2 (10%) and N_2 (89%) was continuously supplied at a space velocity of around $30,000 \text{ h}^{-1}$ ($300 \text{ mL CH}_4 \text{ g}^{-1} \text{ h}^{-1}$) under atmospheric pressure.

Catalytic conversion was evaluated in the 200–600 °C range each 25 °C. The products were analyzed with an on-line gas chromatography (Agilent Technologies 7890N) equipped with thermal conductivity detector (TCD), using a PLOT 5A molecular sieve column (analysis of CH_4 , O_2 , N_2 and CO) and a PLOT U column (CO_2 analysis). The methane conversion is referred to the yield of CO_2 . Kinetic results were checked not to be controlled by both mass and heat transfer limitations, following the criteria proposed by Eurokin [53,54] (see Table S1, Supplementary Material).

4. Conclusions

Three strategies for enhancing the behavior of alumina-supported Co_3O_4 catalysts for oxidation of lean methane were compared. These approaches focused on two main objectives, namely minimizing the formation of inactive cobalt aluminate and promoting the intrinsic activity of the deposited cobalt oxide. Thus, our attention was focused on the surface protection of alumina with magnesia, redox promotion of Co_3O_4 with nickel oxide and surface protection of alumina with ceria, which eventually may also act as a redox promoter for Co_3O_4 . These samples were extensively characterized by WDXRF, BET measurements, XRD, Raman spectroscopy, XPS, H_2 -TPR, CH_4 -TPRe and STEM-EELS/EDX.

Firstly, as for the evaluation of the influence of MgO on the catalytic behavior, magnesia was loaded onto the alumina support prior to Co_3O_4 addition. The incorporation of magnesia hardly affected the textural properties of the blank alumina support, probably due to notable surface area of this promoter. After incorporating cobalt, deposited MgO prevented Co_3O_4 from reacting with the alumina, thereby limiting the generation of inactive cobalt aluminate. On the other hand, a cobalt–magnesium interaction was favored, thereby resulting in better redox properties of the cobalt oxide with a marked shift of the reduction onset temperature by around 30 °C.

Secondly, a bimetallic cobalt-nickel catalyst supported over alumina was synthesized in order to examine the effect of coprecipitating small amounts of nickel (5 wt %) along with the cobalt precursor. The resulting Ni-Co catalyst exhibited good textural properties, with only a slight loss of specific surface with respect to the bare alumina. Combined results from XRD, XPS, Raman spectroscopy and STEM-EELS evidenced that nickel was homogeneously present on the surface and induced the formation of trace amounts of NiCo_2O_4 , because of the partial insertion of Ni^{2+} cation into the lattice of Co_3O_4 . The strong cobalt-nickel interaction promoted the redox properties of the resulting Ni-Co samples. Thus, when compared with the unmodified cobalt catalyst, the reduction onset temperature was noticeably shifted (around 50 °C) to lower temperatures and the specific H_2 uptake in the low temperature range increased to a considerable extent. Furthermore, the higher mobility of active oxygen species over this sample was also evidenced by the temperature-programmed reaction with methane in the absence of gaseous oxygen.

Finally, the cobalt addition over a cerium-coated alumina was examined. Ceria was efficiently dispersed on the support in view of the reduced impact on the textural properties. A dual effect of ceria on the properties of deposited cobalt was evidenced. On one hand, ceria, like magnesia, partially inhibit the formation of undesired cobalt aluminate. More interestingly, a strong interaction between cobalt oxide and ceria was found that ultimately resulted in the insertion of cerium atoms into the spinel lattice of Co_3O_4 . Consequently, a higher abundance of Co^{3+} species at the cost of Co^{2+} was evidenced, thereby promoting the mobility of active lattice oxygen species.

The comparison of the catalytic behavior of the modified catalysts revealed that the most suitable strategy was the addition of cerium to the alumina, prior to the deposition of the cobalt precursor. The resulting optimal catalyst reduced its T_{50} value by 70 °C with respect to the reference catalyst supported over bare alumina, and exhibited a specific reaction rate around three times higher in comparison with the reference Co/Al catalyst.

Supplementary Materials: The following are available online at <http://www.mdpi.com/2073-4344/10/7/757/s1>, Figure S1: CH₄-TPRe profiles of the supported cobalt catalysts, Figure S2: Additional HAADF-STEM images of the Co-Ni/Al (left) and Co/Ce-Al (right) catalysts coupled to EELS (Co (red) and Ni (blue)) and EDX (Co (red) and Ce (green)) elemental distribution, Figure S3: Pseudo-first order fit for the experimental data over the supported cobalt catalysts, Table S1: Series of recommendations and criteria for accurate analysis of intrinsic reaction rates (as evaluated for the Co/Ce-Al catalyst at 400 °C).

Author Contributions: Conceptualization, A.C. and R.L.-F.; Methodology, A.C., B.d.R. and J.I.G.-O.; Formal Analysis, A.C., B.d.R. and R.L.-F.; Investigation, A.C.; Writing—Original Draft Preparation, A.C., B.d.R. and R.L.-F.; Writing—Review and Editing, A.C., J.I.G.-O. and R.L.-F.; Supervision, J.I.G.-O. and R.L.-F.; Funding Acquisition, B.d.R., J.I.G.-O. and R.L.-F. All authors have read and agreed to the published version of the manuscript.

Funding: This research was funded by the Ministry of Economy and Competitiveness (CTQ2016-80253-R AEI/FEDER, UE), Basque Government (IT1297-19) and the University of The Basque Country UPV/EHU (PIF15/335).

Acknowledgments: The author wish to thank the technical and human support provided by SGIker (UPV/EHU) and the Advanced Microscopy Laboratory of the University of Zaragoza.

Conflicts of Interest: The authors declare no conflict of interest.

References

1. Raj, A. Methane emission control. *Johns. Matthey Technol. Rev.* **2016**, *60*, 228–235. [[CrossRef](#)]
2. Khan, M.I.; Yasmin, T.; Shakoor, A. Technical overview of compressed natural gas (CNG) as a transportation fuel. *Renew. Sust. Energy Rev.* **2015**, *51*, 785–797. [[CrossRef](#)]
3. Chen, J.; Arandiyán, H.; Gao, X.; Li, J. Recent advances in catalysts for methane combustion. *Catal. Surv. Asia* **2015**, *19*, 140–171. [[CrossRef](#)]
4. Choudhary, T.V.; Banerjee, S.; Choudhary, V.R. Catalysts for combustion of methane and lower alkanes. *Appl. Catal. A Gen.* **2002**, *234*, 1–23. [[CrossRef](#)]
5. Velin, P.; Ek, M.; Skoglundh, M.; Schaefer, A.; Raj, A.; Thompsett, D.; Smedler, G.; Carlsson, P. Water inhibition in methane oxidation over alumina supported palladium catalysts. *J. Phys. Chem. C* **2019**, *123*, 25724–25737. [[CrossRef](#)]
6. Persson, K.; Pfefferle, L.D.; Schwartz, W.; Ersson, A.; Järås, S.G. Stability of palladium-based catalysts during catalytic combustion of methane: The influence of water. *Appl. Catal. B Environ.* **2007**, *74*, 242–250. [[CrossRef](#)]
7. Hu, J.; Zhao, W.; Hu, R.; Chang, G.; Li, C.; Wang, L. Catalytic activity of spinel oxides MgCr₂O₄ and CoCr₂O₄ for methane combustion. *Mater. Res. Bull.* **2014**, *57*, 268–273. [[CrossRef](#)]
8. Ma, Z. Cobalt oxide catalysts for environmental remediation. *Curr. Catal.* **2014**, *3*, 15–26. [[CrossRef](#)]
9. Pu, Z.; Zhou, H.; Zheng, Y.; Huang, W.; Li, X. Enhanced methane combustion over Co₃O₄ catalysts prepared by a facile precipitation method: Effect of aging time. *Appl. Surf. Sci.* **2017**, *410*, 14–21. [[CrossRef](#)]
10. Zasada, F.; Piskorz, W.; Janas, J.; Grybos, J.; Indyka, P.; Sojka, Z. Reactive oxygen species on the (100) facet of cobalt spinel nanocatalyst and their relevance in ¹⁶O₂/¹⁸O₂ isotopic exchange, *de*N₂O, and *de*CH₄ processes—A theoretical and experimental account. *ACS Catal.* **2015**, *5*, 6879–6892. [[CrossRef](#)]
11. Liotta, L.F.; Wu, H.; Pantaleo, G.; Venezia, A.M. Co₃O₄ nanocrystals and Co₃O₄-MO_x binary oxides for CO, CH₄ and VOC oxidation at low temperatures: A review. *Catal. Sci. Technol.* **2013**, *3*, 3085–3102. [[CrossRef](#)]
12. Liotta, L.F.; Di Carlo, G.; Pantaleo, G.; Venezia, A.M.; Deganello, G. Co₃O₄/CeO₂ composite oxides for methane emissions abatement: Relationship between Co₃O₄-CeO₂ interaction and catalytic activity. *Appl. Catal. B Environ.* **2006**, *66*, 217–227. [[CrossRef](#)]
13. Videla, A.H.M.; Stelmachowski, P.; Ercolino, G.; Specchia, S. Benchmark comparison of Co₃O₄ spinel-structured oxides with different morphologies for oxygen evolution reaction under alkaline conditions. *J. Appl. Electrochem.* **2017**, *47*, 295–304. [[CrossRef](#)]

14. Chen, Z.; Wang, S.; Liu, W.; Gao, X.; Gao, D.; Wang, M.; Wang, S. Morphology-dependent performance of Co_3O_4 via facile and controllable synthesis for methane combustion. *Appl. Catal. A Gen.* **2016**, *525*, 94–102. [[CrossRef](#)]
15. Fei, Z.; He, S.; Li, L.; Ji, W.; Au, C. Morphology-directed synthesis of Co_3O_4 nanotubes based on modified Kirkendall effect and its application in CH_4 combustion. *Chem. Commun.* **2012**, *48*, 853–855. [[CrossRef](#)] [[PubMed](#)]
16. Hu, L.; Peng, Q.; Li, Y. Selective synthesis of Co_3O_4 nanocrystal with different shape and crystal plane effect on catalytic property for methane combustion. *J. Am. Chem. Soc.* **2008**, *130*, 16136–16137. [[CrossRef](#)] [[PubMed](#)]
17. Wang, Q.; Peng, Y.; Fu, J.; Kyzas, G.Z.; Billah, S.M.R.; An, S. Synthesis, characterization, and catalytic evaluation of $\text{Co}_3\text{O}_4/\gamma\text{-Al}_2\text{O}_3$ as methane combustion catalysts: Significance of Co species and the redox cycle. *Appl. Catal. B Environ.* **2015**, *168–169*, 42–50. [[CrossRef](#)]
18. Solsona, B.; Davies, T.E.; Garcia, T.; Vázquez, I.; Dejoz, A.; Taylor, S.H. Total oxidation of propane using nanocrystalline cobalt oxide and supported cobalt oxide catalysts. *Appl. Catal. B Environ.* **2008**, *84*, 176–184. [[CrossRef](#)]
19. Liotta, L.F.; Pantaleo, G.; Macaluso, A.; Di Carlo, G.; Deganello, G. CoO_x catalysts supported on alumina and alumina-baria: Influence of the support on the cobalt species and their activity in NO reduction by C_3H_6 in lean conditions. *Appl. Catal. A Gen.* **2003**, *245*, 167–177. [[CrossRef](#)]
20. Park, S.; Kwak, G.; Lee, Y.; Jun, K.; Kim, Y.T. Effect of H_2O on slurry-phase Fischer–Tropsch synthesis over alumina-supported cobalt catalysts. *Bull. Korean Chem. Soc.* **2018**, *39*, 540–547. [[CrossRef](#)]
21. Park, J.; Yeo, S.; Kang, T.; Heo, I.; Lee, K.; Chang, T. Enhanced stability of Co catalysts supported on phosphorus-modified Al_2O_3 for dry reforming of CH_4 . *Fuel* **2018**, *212*, 77–87. [[CrossRef](#)]
22. Cheng, J.; Yu, J.; Wang, X.; Li, L.; Li, J.; Hao, Z. Novel CH_4 combustion catalysts derived from Cu-Co/X-Al (X = Fe, Mn, La, Ce) hydrotalcite-like compounds. *Energy Fuels* **2008**, *22*, 2131–2137. [[CrossRef](#)]
23. El-Shobaky, H.G.; Shouman, M.A.; Attia, A.A. Effect of La_2O_3 and Mn_2O_3 -doping of $\text{Co}_3\text{O}_4/\text{Al}_2\text{O}_3$ system on its surface and catalytic properties. *Colloids Surf. A Physicochem. Eng. Asp.* **2006**, *274*, 62–70. [[CrossRef](#)]
24. Riad, M. Influence of magnesium and chromium oxides on the physicochemical properties of γ -alumina. *Appl. Catal. A Gen.* **2007**, *327*, 13–21. [[CrossRef](#)]
25. Ulla, M.A.; Spretz, R.; Lombardo, E.; Daniell, W.; Knözinger, H. Catalytic combustion of methane on Co/MgO: Characterisation of active cobalt sites. *Appl. Catal. B Environ.* **2001**, *29*, 217–229. [[CrossRef](#)]
26. Ji, S.; Ji, S.; Wang, H.; Flahaut, E.; Coleman, K.S.; Green, M.L.H. Catalytic combustion of methane over cobalt-magnesium oxide solid solution catalysts. *Catal. Lett.* **2001**, *75*, 65–71. [[CrossRef](#)]
27. Trivedi, S.; Prasad, R. Selection of cobaltite and effect of preparation method of NiCo_2O_4 for catalytic oxidation of CO– CH_4 mixture. *Asia-Pac. J. Chem. Eng.* **2017**, *12*, 440–453. [[CrossRef](#)]
28. Lim, T.H.; Cho, S.J.; Yang, H.S.; Engelhard, M.H.; Kim, D.H. Effect of Co/Ni ratios in cobalt nickel mixed oxide catalysts on methane combustion. *Appl. Catal. A Gen.* **2015**, *505*, 62–69. [[CrossRef](#)]
29. Dumond, F.; Marceau, E.; Che, M. A study of cobalt speciation in $\text{Co}/\text{Al}_2\text{O}_3$ catalysts prepared from solutions of cobalt-ethylenediamine complexes. *J. Phys. Chem. C* **2007**, *111*, 4780–4789. [[CrossRef](#)]
30. Pérez-Ramírez, J.; Mul, G.; Kapteijn, F.; Moulijn, J.A. In situ investigation of the thermal decomposition of Co-Al hydrotalcite in different atmospheres. *J. Mater. Chem.* **2001**, *11*, 821–830. [[CrossRef](#)]
31. Marco, J.F.; Gancedo, J.R.; Gracia, M.; Gautier, J.L.; Ríos, E.; Berry, F.J. Characterization of the nickel cobaltite, NiCo_2O_4 , prepared by several methods: An XRD, XANES, EXAFS, and XPS study. *J. Solid State Chem.* **2000**, *153*, 74–81. [[CrossRef](#)]
32. Lukashuk, L.; Yigit, N.; Rameshan, R.; Kolar, E.; Teschner, D.; Hävecker, M.; Knop-Gericke, A.; Schlögl, R.; Föttinger, K.; Rupprechter, G. Operando insights into CO oxidation on cobalt oxide catalysts by NAP-XPS, FTIR, and XRD. *ACS Catal.* **2018**, *8*, 8630–8641. [[CrossRef](#)] [[PubMed](#)]
33. Dupin, J.; Gonbeau, D.; Vinatier, P.; Lévassieur, A. Systematic XPS studies of metal oxides, hydroxides and peroxides. *Phys. Chem. Chem. Phys.* **2000**, *2*, 1319–1324. [[CrossRef](#)]
34. Wu, L.; Jiao, D.; Wang, J.; Chen, L.; Cao, F. The role of MgO in the formation of surface active phases of $\text{CoMo}/\text{Al}_2\text{O}_3\text{-MgO}$ catalysts for hydrodesulfurization of dibenzothiophene. *Catal. Commun.* **2009**, *11*, 302–305. [[CrossRef](#)]
35. Cazzanelli, E.; Kuzmin, A.; Mariotto, G.; Mironova-Ulmane, N. Study of vibrational and magnetic excitations in $\text{Ni}_x\text{Mg}_{1-x}\text{O}$ solid solutions by Raman spectroscopy. *J. Phys. Condens. Matter* **2003**, *15*, 2045–2052. [[CrossRef](#)]

36. Trivedi, S.; Prasad, R.; Gautam, S.K. Design of active NiCo₂O_{4-δ} spinel catalyst for abatement of CO-CH₄ emissions from CNG fueled vehicles. *AIChE J.* **2018**, *64*, 2632–2646. [[CrossRef](#)]
37. Pettiti, I.; Gazzoli, D.; Benito, P.; Fornasari, G.; Vaccari, A. The reducibility of highly stable Ni-containing species in catalysts derived from hydrotalcite-type precursors. *RSC Adv.* **2015**, *5*, 82282–82291. [[CrossRef](#)]
38. Zasada, F.; Grybos, J.; Budiyanto, E.; Janas, J.; Sojka, Z. Oxygen species stabilized on the cobalt spinel nano-octahedra at various reaction conditions and their role in catalytic CO and CH₄ oxidation, N₂O decomposition and oxygen isotopic exchange. *J. Catal.* **2019**, *371*, 224–235. [[CrossRef](#)]
39. Zasada, F.; Janas, J.; Piskorz, W.; Gorczynska, M.; Sojka, Z. Total oxidation of lean methane over cobalt spinel nanocubes controlled by the self-adjusted redox state of the catalyst: Experimental and theoretical account for interplay between the Langmuir-Hinshelwood and Mars-Van Krevelen mechanisms. *ACS Catal.* **2017**, *7*, 2853–2867. [[CrossRef](#)]
40. Choya, A.; de Rivas, B.; González-Velasco, J.R.; Gutiérrez-Ortiz, J.I.; López-Fonseca, R. Oxidation of residual methane from VNG vehicles over Co₃O₄-based catalysts: Comparison among bulk, Al₂O₃-supported and Ce-doped catalysts. *Appl. Catal. B Environ.* **2018**, *237*, 844–854. [[CrossRef](#)]
41. Zheng, Y.; Yu, Y.; Zhou, H.; Huang, W.; Pu, Z. Combustion of lean methane over Co₃O₄ catalysts prepared with different cobalt precursors. *RSC Adv.* **2020**, *10*, 4490–4498. [[CrossRef](#)]
42. Liotta, L.F.; Di Carlo, G.; Pantaleo, G.; Deganello, G. Catalytic performance of Co₃O₄/CeO₂ and Co₃O₄/CeO₂-ZrO₂ composite oxides for methane combustion: Influence of catalyst pretreatment temperature and oxygen concentration in the reaction mixture. *Appl. Catal. B Environ.* **2007**, *70*, 314–322. [[CrossRef](#)]
43. Ji, Y.; Zhao, Z.; Duan, A.; Jiang, G.; Liu, J. Comparative study on the formation and reduction of bulk and Al₂O₃-supported cobalt oxides by H₂-TPR technique. *J. Phys. Chem. C* **2009**, *113*, 7186–7199. [[CrossRef](#)]
44. de Rivas, B.; Sampedro, C.; Ramos-Fernández, E.V.; López-Fonseca, R.; Gascon, J.; Makkee, M.; Gutiérrez-Ortiz, J.I. Influence of the synthesis route on the catalytic oxidation of 1,2-dichloroethane over CeO₂/H-ZSM5 catalysts. *Appl. Catal. A Gen.* **2013**, *456*, 96–104. [[CrossRef](#)]
45. Huang, Y.; Fan, W.; Long, B.; Li, H.; Qiu, W.; Zhao, F.; Tong, Y.; Ji, H. Alkali-modified non-precious metal 3D-NiCo₂O₄ nanosheets for efficient formaldehyde oxidation at low temperature. *J. Mater. Chem. A* **2016**, *4*, 3648–3654. [[CrossRef](#)]
46. Genty, E.; Siffert, S.; Cousin, R. Investigation of reaction mechanism and kinetic modelling for the toluene total oxidation in presence of CoAlCe catalyst. *Catal. Today* **2019**, *333*, 28–35. [[CrossRef](#)]
47. Bahlawane, N. Kinetics of methane combustion over CVD-made cobalt oxide catalysts. *Appl. Catal. B Environ.* **2006**, *67*, 168–176. [[CrossRef](#)]
48. Stefanov, P.; Todorova, S.; Naydenov, A.; Tzaneva, B.; Kolev, H.; Atanasova, G.; Stoyanova, D.; Karakirova, Y.; Aleksieva, K. On the development of active and stable Pd-Co/γ-Al₂O₃ catalyst for complete oxidation of methane. *Chem. Eng. J.* **2015**, *266*, 329–338. [[CrossRef](#)]
49. Paredes, J.R.; Díaz, E.; Díez, F.V.; Ordóñez, S. Combustion of methane in lean mixtures over bulk transition-metal oxides: Evaluation of the activity and self-deactivation. *Energy Fuels.* **2009**, *23*, 86–93. [[CrossRef](#)]
50. Choya, A.; de Rivas, B.; Gutiérrez-Ortiz, J.I.; López-Fonseca, R. Effect of residual Na⁺ on the combustion of methane over Co₃O₄ bulk catalysts prepared by precipitation. *Catalysts* **2018**, *8*, 427. [[CrossRef](#)]
51. Choya, A.; de Rivas, B.; González-Velasco, J.R.; Gutiérrez-Ortiz, J.I.; López-Fonseca, R. Oxidation of lean methane over cobalt catalysts supported on ceria/alumina. *Appl. Catal. A Gen.* **2020**, *591*, 117381. [[CrossRef](#)]
52. Choya, A.; de Rivas, B.; González-Velasco, J.R.; Gutiérrez-Ortiz, J.I.; López-Fonseca, R. On the beneficial effect of MgO promoter on the performance of Co₃O₄/Al₂O₃ catalysts for combustion of dilute methane. *Appl. Catal. A Gen.* **2019**, *582*, 117099. [[CrossRef](#)]
53. EUROKIN Spreadsheet on Requirements for Measurement of Intrinsic Kinetics in the Gas-Solid Fixed-Bed Reactor. Available online: <http://eurokin.org/> (accessed on 29 April 2020).
54. Aranzabal, A.; González-Marcos, J.A.; Ayastuy, J.L.; González-Velasco, J.R. Kinetics of Pd/alumina catalysed 1,2-dichloroethane gas-phase oxidation. *Chem. Eng. Sci.* **2006**, *61*, 3564–3576. [[CrossRef](#)]

